Full Paper

Journal of the Brazilian Chemical Society

https://dx.doi.org/10.21577/0103-5053.20260022

J. Braz. Chem. Soc. **2026**, *37*, e-20260022, 1-17

Study of the Photoassisted Sonoelectrochemical Process for Degradation of the Pesticides Ametryn, Diuron and Hexazinone

Karla S. de Araújo,[a] Beatriz Sugahara,[b] Marquele A. Tonhela,[a] Maria Emilia Veloso,[b] Mateus S. Freitas,[c] Ana Claudia Granato,[b,c] Ana Letícia S. Abrão,[d] Deusmaque C. Ferreira[d] and Geoffroy Roger P. Malpass[*,a,b,c,d]

[a]*Programa Multicêntrico de Pós-Graduação em Química de Minas Gerais (PPGMQ-MG), Universidade Federal do Triângulo Mineiro, 38064-200 Uberaba-MG, Brazil*

[b]*Departamento de Engenharia Química, Universidade Federal do Triângulo Mineiro, 38064-200 Uberaba-MG, Brazil*

[c]*Programa de Mestrado Profissional em Inovações e Tecnologias (PMPIT), Universidade Federal do Triângulo Mineiro, 38064-200 Uberaba-MG, Brazil*

[d]*Programa de Pós-Graduação em Ciência e Tecnologia Ambiental (PPGCTA), Universidade Federal do Triângulo Mineiro, 38064-200 Uberaba-MG, Brazil*

Water contamination from pesticides in industrial and agricultural effluents has significant environmental impacts, necessitating the development of effective treatment technologies. This article discusses the use of a combined electrochemical, photochemical, and sonochemical approach to degrade pesticides like ametryn, diuron, and hexazinone. A bench-scale electrochemical flow reactor with a $Ti/Ru_{0.3}Ti_{0.7}O_2$ anode, Ti counter-electrode, and NaCl as the electrolyte was utilized. Process optimization involved varying electric current and NaCl concentration, with free chlorine species (FCS) production as the response variable. Optimal conditions were achieved at 0.88 mol L^{-1} [NaCl] and 0.78 A current. This photoassisted sonoelectrochemical process effectively degraded the pesticides, achieving total organic carbon (TOC) removal rates of 91, 94, and 77% for ametryn, diuron, and hexazinone, respectively. High-performance liquid chromatography (HPLC) analysis showed near-total removal for ametryn and diuron and 80.7% for hexazinone. Kinetic studies indicated that the degradation followed a pseudo-first-order model, with rate constants increasing approximately 1.8-2.5 times under the combined process compared to the electrochemical method. Additionally, this triple-combined approach enhanced current efficiency, reduced energy use, and improved overall system energy efficiency, proving to be an effective and promising treatment method.

Keywords: emerging contaminants, effluents, electrochemistry, free chlorine species, experimental design, advanced oxidative processes (AOPs)

Introduction

Pesticides are substances designed to control pests, including insects, plant pathogens, weeds, nematodes, rodents, and fungi.[1] Pesticides can be classified according to their target pest (e.g., herbicides, insecticides, or fungicides) or their chemical structure (such as organochlorines and carbamates). Due to their widespread use, pesticides can contaminate various environmental compartments, including soil and water, raising significant concerns regarding food and environmental safety.[1-3]

It is important to note that not only the active ingredients are of concern but also the auxiliary components (also known as co-formulants or adjuvants) present in pesticide formulations. These components, used to enhance solubility, dispersion, and environmental persistence, may exert their own adverse effects and increase the penetration of active ingredients into non-target organisms, including humans.[4-6] Recent studies[4,7,8] indicate that complete pesticide formulations, and not only their active ingredients, should be considered in

*e-mail: geoffroy.malpass@uftm.edu.br
Editor handled this article: Cristiane Luísa Jost (Associate)

risk assessments, as they may contain substances such as PFAS (per- and polyfluoroalkyl substances) and exhibit synergistic or additive toxicity.

Pesticide contamination occurs on a global scale, with reports indicating that pesticide residues can be detected in numerous water bodies.[9,10] It is noteworthy that the presence of these contaminants in aquatic environments can cause severe water pollution even at very low concentrations (ranging from 1 ng L^{-1} to 1 μg L^{-1}), with the potential for biomagnification through the food chain.[11,12]

The conservation of water resources is a critical global issue that represents an ongoing challenge for the scientific community. Therefore, it is imperative to implement wastewater treatment technologies-both for industrial and agricultural effluents-that not only degrade but also eliminate pesticide residues.[13-15]

However, conventional water and wastewater treatment methods, such as activated sludge, coagulation-flocculation, and sedimentation, present limitations in removing recalcitrant micropollutants like pesticides. Biological processes can be inhibited by the toxicity or low biodegradability of these compounds, resulting in insufficient mineralization rates. Physical separation techniques, such as adsorption onto activated carbon, while effective in retention, only transfer the contaminant from one phase to another (water to solid), generating saturated residues that require complex disposal or regeneration. Furthermore, conventional chemical oxidation, such as chlorination, can lead to the formation of organochlorine byproducts potentially more toxic than the original molecules. These restrictions highlight the need for alternative technologies capable of effectively degrading such contaminants.[16,17]

In this context, advanced oxidation processes (AOPs) are well-established technologies for treating effluents containing pesticides.[18-20] These methods can be applied individually or in combination with one another or with other treatment technologies. The principle of AOPs lies in the partial or complete conversion of contaminants into simpler species such as water (H_2O), carbon dioxide (CO_2), inorganic anions, or less toxic substances that are more easily degraded by conventional treatment processes.[18-20]

The advantages of AOPs are numerous. They provide a strong oxidative potential and operate under ambient temperature and pressure. AOPs can achieve the mineralization and total oxidation of both organic pollutants and inorganic species. They are versatile and efficient, being able to completely mineralize various classes of pollutants, including refractory compounds. For instance, recent studies[21,22] have demonstrated the high efficiency of AOPs in treating effluents contaminated with pesticides.

Some studies have achieved remarkable results in the removal of contaminants from aqueous effluents by combining electrochemical and photochemical methods-known as photoassisted electrochemical oxidation.[23-25] However, few studies have explored the combined application of electrochemical (EC), photochemical (UV), and sonochemical (US) techniques for pesticide degradation.

In the literature, studies usually only study up to two AOPs at a time - typically electrochemical-photochemical or electrochemical-sonochemical approaches - without integrating all three into a single continuous-flow system. For example, Martínez-Sánchez *et al*.[23] reported electrochemical AOPs coupled with UV irradiation for pesticide removal, while Deshmukh and Deosarkar[24] evaluated ultrasound-photocatalysis hybrids, and Peralta-Hernández *et al*.[18] focused exclusively on electrochemical and photoassisted configurations. None of these studies incorporated simultaneous electrochemical, photochemical and sonochemical activation in a single reactor.

Recent investigations, including the work of Tonhela *et al*.,[26] have demonstrated the effectiveness of photoassisted sonoelectrochemical systems in the mineralization of recalcitrant compounds, with notable reductions in energy demand attributed to the simultaneous activation by UV radiation and ultrasound. In a similar context, Yadav *et al*.[1] reported improved degradation efficiencies for persistent pharmaceutical contaminants through hybrid approaches that combine anodic oxidation with statistically optimized Fenton processes. Collectively, these studies highlight a prevailing trend toward the integration of AOPs as a strategy to mitigate mass transfer limitations and enhance the generation of hydroxyl radicals (•OH) and active chlorine species. Although fully integrated systems remain limited, the recent literature reflects a growing interest in exploiting the synergistic effects between electrochemical methods[27] and other oxidative technologies for the treatment of emerging contaminants.

Thus, the novelty of this study lies in the integrated evaluation of a continuous-flow photoassisted sonoelectrochemical system for the simultaneous degradation of the pesticides ametryn, diuron, and hexazinone. Unlike previous works that focus on isolated or binary techniques, this study employs a central composite design (CCD) to optimize the coupling of electrochemical, photochemical, and sonochemical processes. This approach aims to maximize the generation of active chlorine species and assess the synergistic efficiency of the triple-combined system in a flow reactor setup, filling a gap in the literature regarding the treatment of complex herbicide mixtures.

Experimental

Electrochemical reactor and system configuration

The system was assembled using a filter-press type electrochemical reactor operating in batch recirculation mode. The electrolyte solution was continuously pumped from an external reservoir (capacity = 250 cm^3) through the reactor cell using a peristaltic pump (Cole-Parmer, 07554-90) at a fixed flow rate of 5 mL s^{-1}.

The reactor cell accommodates a commercial $Ti/Ru_{0.3}Ti_{0.7}O_2$ Dimensionally Stable Anode (DSA®, De Nora Brazil) as the anode and a titanium (Ti) mesh as the cathode. Both electrodes have a constant exposed geometric area of 2 cm^2 and are separated by an inter-electrode gap of 3 cm using Viton and Teflon spacers.[28] The electric current was supplied by a stabilized current source (Minipa do Brasil Ltda, MPL-1303M) and monitored with a digital multimeter (Minipa ET-2076).

Coupled AOPs configuration

To enable the photoassisted processes, the reactor is equipped with a quartz window positioned parallel to the anode surface. This configuration allows the UV radiation from the high-pressure Hg lamp (Osram, 375 W, λ_{max} = 254 nm) to penetrate the cell and directly illuminate the electrode surface, ensuring homogeneous irradiation of the reaction zone at an intensity of 8.4 mW cm^{-2}. The UV lamp was placed within a dark chamber to prevent light loss and all photochemical and photoassisted experiments were conducted under identical irradiation geometry.

Sonochemical and sonoelectrochemical experiments were performed using an ultrasonic bath (Cristófoli, Brazil) operating at 42 kHz and 60 W in continuous mode. The reaction reservoir was partially immersed at a constant depth to ensure reproducible acoustic coupling, resulting in an estimated ultrasonic power density of 0.03 W cm^{-2}. The solution temperature was monitored during sonication and remained below 30 °C, minimizing thermal effects on degradation kinetics.

The combined photoassisted sonoelectrochemical experiments (EC/UV/US) were conducted by simultaneously applying electric current, UV irradiation, and ultrasonic energy, maintaining the same fluid dynamics configuration. All operational parameters, including the inter-electrode gap, flow rate, light intensity, and ultrasonic power density, were standardized across all individual and combined experiments to allow for a direct comparison of the degradation kinetics and synergistic effects. The configuration employed in this study has been fully presented and validated in previous publications.[26] A schematic representation of the integrated system is provided in Figure 1. For a more detailed presentation of the electrochemical reactor, readers are directed to other studies from the laboratory.[29,30]

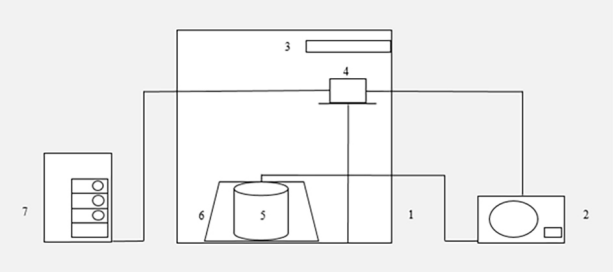

Figure 1. Schematic representation of the continuous-flow photoassisted sonoelectrochemical system used in this study: (1) dark chamber; (2) peristaltic pump (5 mL s^{-1}); (3) high-pressure Hg UV lamp (375 W, 8.4 mW cm^{-2}); (4) electrochemical filter-press cell equipped with a $Ti/Ru_{0.3}Ti_{0.7}O_2$ (DSA®) anode and Ti cathode (geometric area = 2 cm^2, inter-electrode gap = 3 cm); (5) electrolyte reservoir (250 mL); (6) ultrasonic bath (42 kHz, 60 W); and (7) stabilized DC power supply. NaCl was used as supporting electrolyte.

Materials and reagents

All regents used were of ACS grade and were used without further purification. The pesticide samples were provided by a local company and were of commercial grade (> 99%).

Total organic carbon (TOC) monitoring, kinetic evaluation, and energetic analysis

The mineralization of the pesticides ametryn, diuron, and hexazinone was monitored by total organic carbon (TOC) analysis throughout all individual and combined advanced oxidation processes. TOC data were used to quantify the degradation kinetics under each operational mode. Assuming pseudo-first-order behavior, the kinetic constant (k) was obtained by fitting the concentration profiles to the differential rate expression, as given in equation 1:

$$\frac{dC}{dt} = -kC \quad (1)$$

where C is the TOC concentration and t the reaction time. To evaluate the performance of the combined photoassisted sonoelectrochemical process relative to the isolated electrochemical, photochemical, and sonochemical routes, a synergistic coefficient (Sc) was calculated according to Choi *et al.*[31] and Weng *et al.*[32] (as given in equation 2):

$$Sc = \frac{k4}{k_1 + k_2 + k_3} \quad (2)$$

where k_1, k_2 and k_3 correspond to the electrochemical, photochemical, and sonochemical processes, respectively, and k_4 represents the rate constant obtained for the triple-combined system.

Because all degradation processes followed pseudo-first-order kinetics, the electric energy *per* order (E_{EO})[33,34] was determined to compare energetic feasibility among operational modes. The E_{EO} (equation 3) expresses the electrical energy required to reduce contaminant concentration by one order of magnitude and was calculated as:

$$E_{EO} = \frac{P_{el} t}{V \log\left(\frac{TOC_i}{TOC_f}\right)} \quad (3)$$

where P_{el} is the applied electrical power including photochemical and sonochemical systems (kW), V is the reactor volume (L), t is the reaction time (h), and TOC_i and TOC_f denote the initial and final TOC values.

In addition to the kinetic assessment, a detailed energetic evaluation was performed for all processes involving electrolysis. Current efficiency (CE) was first calculated to determine the fraction of applied charge effectively used for mineralization (equation 4):

$$CE = \frac{2.67(TOC_i - TOC_f)FV}{it} \quad (4)$$

where F is the Faraday constant (96487 C mol^{-1}), i the applied current (A), V the treated volume (L), and t the electrolysis time (s). Energy consumption (EC) was then obtained using equation 5:

$$EC = \frac{iUt1000}{V} \quad (5)$$

with U being the cell potential (V) and V expressed in m^3.

Energy efficiency (EE) was determined from the charge associated with free chlorine species (FCS) formation. The charge related to chlorine generation (Q_{Cl}) was calculated using equation 6:

$$Q_{Cl} = \frac{m_{Cl}}{mMM_{Cl}} Qe \quad (6)$$

where m_{Cl} corresponds to the chlorine mass in a 250 mL aliquot, MM_{Cl} is the molar mass of Cl_2 (70.9 g mol^{-1}), and Q_e the electron charge for the Cl^-/Cl_2 reaction (1.93×10^5 C). The total charge passed during electrolysis (Q_T) was obtained from equation 7:

$$Q_T = it \quad (7)$$

Finally, energy efficiency (EE) was calculated from equation 8:

$$EE = \frac{QCl}{QT} \quad (8)$$

This parameter quantifies the proportion of electrical energy effectively converted into oxidizing chlorine species during the electrochemical step. All experiments were conducted under identical hydrodynamic and operational conditions to enable direct comparison across individual and coupled AOPs.

Procedures

Initially, the production of free chlorine species (FCS) and energy efficiency were studied using a 2^2 factorial design, with current (0.10-0.40 A) and NaCl concentration (0.05-0.60 mol L^{-1}) as variables, at a constant reaction time of 30 min. Optimization was subsequently performed using a central composite design (CCD) to determine the maximum response point for FCS production ($HOCl/OCl^-$). In this part of the study, only the purely electrochemical method was employed, as it is the sole approach that generates FCS.

Current intensity was selected as the independent variable instead of current density (50 mA cm^{-2}) because the geometric area of the working electrode remained constant (2 cm^2) throughout all experiments. Consequently, variations in current intensity are directly proportional to current density. For comparative purposes, the applied currents of 0.10 and 0.40 A correspond to current densities of 50 and 200 mA cm^{-2}, respectively. This approach aligns with the methodology reported by Tonhela *et al.*,[26] ensuring consistent optimization parameters for this reactor configuration.

Subsequently, degradation assays were performed using ametryn, diuron, and hexazinone solutions prepared in ultrapure water (Milli-Q) at an initial concentration of 20 mg L^{-1}, chosen to simulate levels found in local fertilizer industry effluents. The optimized NaCl concentration 0.88 mol L^{-1} determined by the CCD was used as the supporting electrolyte. The reactor operated in batch recirculation mode with a total reaction volume of 250 mL. All individual (electrochemical, photochemical,

sonochemical) and combined hybrid processes were conducted for a total time of 60 min. Aliquots were withdrawn at pre-established intervals (0; 5; 10; 20; 30; 45 and 60 min) to monitor pesticide concentration decay, pH evolution, and mineralization (TOC).

Analysis

Free chlorine species (as HOCl/OCl$^-$) concentrations were determined by the iodometric titration method.[26] To identify/analyze the regions of greater absorption, as well as detect the presence of FCS, the samples were analyzed using UV spectroscopy (PerkinElmer, UV-Vis Spectrometer), recorded in the 200-400 nm range with a resolution of 1 nm, using ultrapure water as reference and averaging three consecutive scans *per* measurement.

To check the pH of the treated solutions and confirm the presence of FCS, pH analysis was performed using a pH meter (HANNA instruments HI3221 pH|ORP|ISE meter), calibrated by buffer solutions of pH = 4 and pH = 7.[26] UV-Vis analyses were carried out using a PerkinElmer spectrophotometer with quartz cuvettes (optical path length = 1.0 cm). Spectra were recorded in the 200-400 nm range with a resolution of 1 nm, using ultrapure water as reference and averaging three consecutive scans *per* measurement.

The concentration of ametryn and diuron was determined by high performance liquid chromatography (HPLC; Shimadzu, LCSolution Multi-PDA) using a Shim-pack 5µ C18 reversed-phase column (150 × 4.60 mm). For ametryn, the method was adapted from Brondi and Lanças,[35] and the mobile phase was composed of a mixture of water: acetonitrile (70:30% v/v) operated in isocratic mode, with a flow rate of 0.7 mL min^{-1}, temperature of 31 °C, injection volume of 20 µL, detection at 238 nm and a retention time of 5.20 min. For diuron the mobile phase was composed of a mixture of acetonitrile:water (45:155% v/v) operated in isocratic mode, with a flow rate of 0.86 mL min^{-1}, injection volume of 20 µL, detection at 249 nm and time retention time of 8.76 min, and was adapted from the work Brondi and Lanças[35] and Felicio *et al.*[36] The analysis of hexazinone was an adaptation of the method used by Brondi and Lanças,[35] using reverse phase LiChrosPher 5µ RP-18 column (150 × 4.00 mm) (PHENOMENEX) at room temperature (25 °C), the mobile phase being composed of a mixture of acetonitrile:water (28:72% v/v) operated in isocratic mode, with a flow rate of 0.7 mL min^{-1}, injection volume of 20 µL, detection at 244 nm and retention time of 7.58 min.

TOC analysis was employed to monitor the percentage of mineralization before and after each treatment (Shimadzu, TOC-LCSH, ASI-L) to assess the total removal of organic compounds present.

Results and Discussion

Factorial planning 2^2

The initial factorial design (2^2) was performed to verify the significant variables for the monitored response, i.e., the maximum production of FCS. As previously stated, the studied variables were electrolyte (NaCl) concentration (0.05-0.60 mol L^{-1}) and applied current (0.10-0.40 A). Table 1 presents the values obtained for the response variable (FCS) of the 2^2 factorial design with replicates.

Considering the data presented in Table 1, the Pareto chart (Figure 2) presents the most significant effects (in descending order) on the process ([NaCl] and current) for

Table 1. Experimental matrix and response values obtained from the 2^2 factorial design for free chlorine species (FCS) production as a function of NaCl concentration and applied current. FCS corresponds to the sum of hypochlorous acid and hypochlorite ions (HOCl/OCl$^-$). Experiments were performed in duplicate under identical hydrodynamic conditions (flow rate = 5 mL s^{-1}; reaction time = 30 min)

Experiment	Replica	[NaCl] / (mol L^{-1})	Current / A	FCS / (mg L^{-1})
1	2	0.60 (+1)	0.40 (+1)	992.60
2	1	0.60 (+1)	0.40 (+1)	1005.30
3	2	0.60 (+1)	0.10 (−1)	365.14
4	1	0.60 (+1)	0.10 (−1)	380.76
5	1	0.05 (−1)	0.40 (+1)	219.05
6	2	0.05 (−1)	0.40 (+1)	202.07
7	2	0.05 (−1)	0.10 (−1)	293.60
8	1	0.05 (−1)	0.10 (−1)	309.69

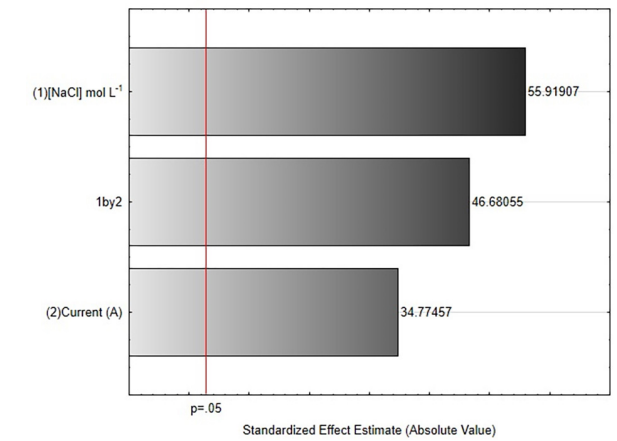

Figure 2. Pareto chart showing the standardized effects of NaCl concentration, applied current, and their interaction on free chlorine species (FCS) production in the 2^2 factorial design. The vertical dashed line indicates the 95% confidence level (p = 0.05).

FCS production. The threshold of the 95% significance level is indicated by the vertical dashed line. From Figure 2 it can be observed that there is a positive effect for the variation of [NaCl] and current and for the interaction [NaCl]/current.

The positive variation observed in Figure 2 with respect to NaCl concentration can be explained by the fact that higher chloride concentrations promote greater generation of active chlorine species, such as hypochlorite and hypochlorous acid (FCS, HOCl/OCl$^-$). This behavior is consistent with similar electrochemical systems, in which increasing NaCl concentration enhances the electrolysis rate and, consequently, the production of active chlorine. For example, Afify *et al.*[37] demonstrated that hypochlorite production in saline wastewater increases with NaCl concentration when using porous graphite electrodes. Similarly, Lee and Kim[38] observed that higher chloride concentrations improve the efficiency of hypochlorite ion generation in electrochemical cells, while Rodríguez and Nava[39] reported a positive effect of diluted chloride concentration on active chlorine synthesis. Moreover, Medina Collana[40] showed that NaCl concentration directly influences current and the generation of active chlorine species in electrolytic cells, and Kamel *et al.*[41] indicated that both additives and electrode roughness can modulate this effect, reinforcing the observed increase in FCS production at higher NaCl concentrations.

It is also observed that the applied current exerts a positive influence on the generation of active chlorine species, although less pronounced than that of NaCl concentration. This behavior is expected, as the applied current is directly related to energy consumption in the electrochemical process. Recent studies support this relationship: Janowski *et al.*[42] emphasized that electrical energy consumption is a key criterion for rationalizing the application of electrochemical processes, considering that electricity is the main energy source. Furthermore, Faria *et al.*[43] observed that modulation of the applied current can optimize electrochemical oxidation, indicating that the current directly influences the process energy efficiency. Therefore, the applied current should be carefully balanced to maximize energy efficiency without compromising process effectiveness.

Studies also indicate that applying electric current in continuous-flow electrochemical cells enhances mass transfer, thereby optimizing process efficiency. For instance, Pose-Juan *et al.*[44] demonstrated that continuous-flow electrochemical reactors improve mass transfer by increasing the electrode area-to-volume ratio, achieving good performance in wastewater treatment. Similarly, Klement *et al.*[45] highlighted that continuous-flow reactors are highly promising for electrochemical conversions, largely due to the rapid replenishment of reagents, which facilitates mass transfer.

The response surface and contour plots are presented in Figure 3. Both graphs reinforce the conclusions drawn from Figure 2 regarding the effects of the studied variables: the higher the [NaCl] concentration and applied current, the greater the response variable value. This indicates that increasing [NaCl] and current enhances the production of free chlorine species (HOCl/OCl$^-$), with [NaCl] having the stronger influence.

Central composite design (CCD)

The results obtained from the 2^2 factorial design were used to perform the subsequent CCD, generating an experimental matrix with 11 experiments, including one repetition at the central point. Table 2 presents the CCD results, considering the experiments and repetitions for the production of FCS as the response variable.

The Pareto chart (Figure 4) shows that the quadratic term of [NaCl] was the most significant effect at a 95%

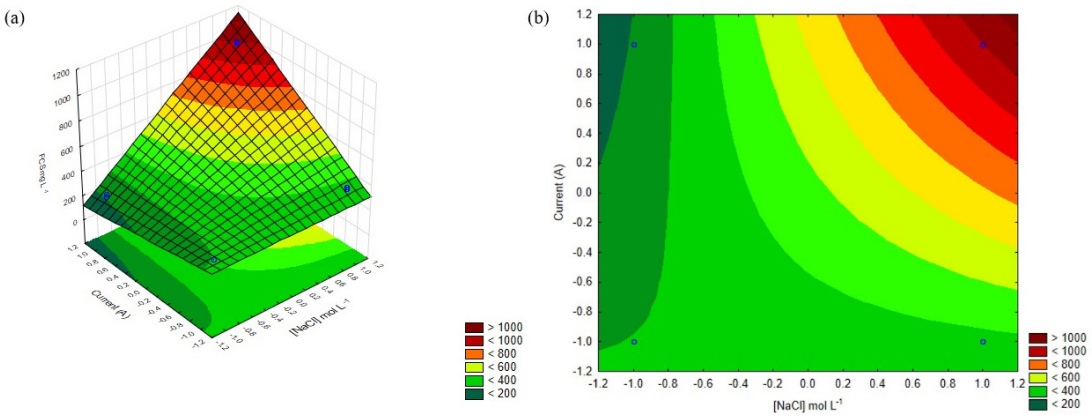

Figure 3. Influence of NaCl concentration and applied current on free chlorine species (FCS) production obtained from the 2^2 factorial design: (a) response surface and (b) contour plot. FCS corresponds to the sum of HOCl/OCl$^-$ generated during electrolysis.

Table 2. Central composite design (CCD) matrix and experimental results for free chlorine species (FCS) production as a function of NaCl concentration and applied current. FCS is expressed as the combined concentration of HOCl and OCl^-. The central point was performed in triplicate to estimate experimental error

Experiment	[NaCl] / (mol L^{-1})	Applied current / A	FCS / (mg L^{-1})
1	0.28 (−1)	0.15 (−1)	389.95
2	1.15 (+1)	0.15 (−1)	779.90
3	0.28 (−1)	0.70 (+1)	1098.95
4	1.15 (+1)	0.70 (+1)	1145.04
5	0.88 (0)	0.16 (−α)[a]	1251.39
6	0.88 (0)	0.94 (+α)[a]	2658.75
7	0.26 (−α)[a]	0.55 (0)	932.34
8	1.49 (+α)[a]	0.55 (0)	1230.12
9	0.88 (0)	0.55 (0)	2279.44
10	0.88 (0)	0.55 (0)	2113.25
11	0.88 (0)	0.55 (0)	2243.99

[a]α (alpha) is the axial (or star) distance used in a central composite design (CCD).

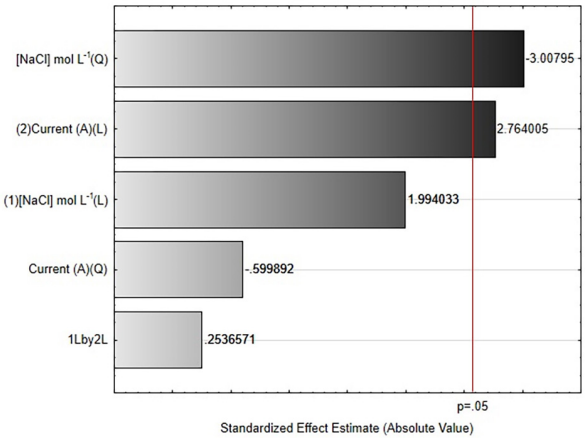

Figure 4. Pareto chart obtained from the central composite design (CCD) indicating the significant linear and quadratic effects of NaCl concentration and applied current on FCS production at a 95% confidence level.

confidence level, exhibited a negative influence on the process. The linear term of the applied current showed a positive influence, that is, the higher the applied current, the greater the production of FCS. The interaction terms between the variables were not significant at the 95% confidence level.

The response surface and contour plots are presented in Figure 5 to evaluate the influence of [NaCl] concentration and applied current. It can be observed that a greater amount of FCS is produced when both [NaCl] concentration and applied current are increased.

The critical point and the observed minimum and maximum values are presented in Table 3. As can be seen, the optimal condition for FCS production was achieved at 0.88 mol L^{-1} of [NaCl] and 0.78 A of applied current. Subsequently, this optimal condition (maximum FCS production) was applied to the degradation of the pesticides ametryn, diuron, and hexazinone.

Table 3. Minimum, maximum, and critical point values of NaCl concentration and applied current obtained from the central composite design optimization for maximum free chlorine species (FCS) production.

Factor	Minimum	Critical point	Maximum
[NaCl] / (mol L^{-1})	0.26	0.88	1.49
Current / A	0.15	0.78	0.94

ANOVA of process performance

Analysis of variance (ANOVA) is a statistical technique that compares the variability between groups with the variability within groups to determine whether there are differences between the group mean values. A well-fitted model is indicated when the associated *p*-value is lower than the significance level (< 0.05). The ANOVA results (Tables S1, S2, S3 in the Supplementary Information (SI) section) show that treatment type had a highly significant

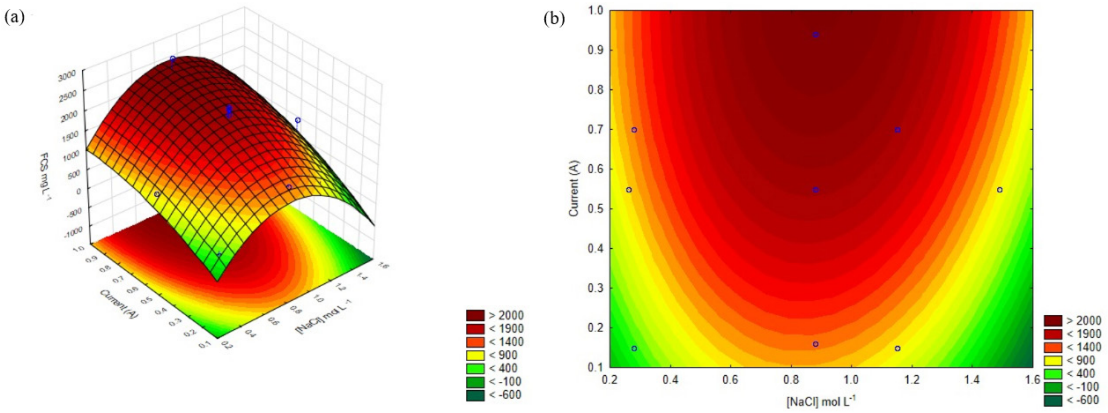

Figure 5. Response surface (a) and contour plot (b) derived from the CCD, illustrating the combined effect of NaCl concentration and applied current on free chlorine species ($HOCl/OCl^-$) generation under electrochemical conditions.

effect on all performance metrics ($p < 0.000001$), confirming that differences among the electrochemical, photoassisted, sonoelectrochemical, and photoassisted-sonoelectrochemical processes are statistically robust. Overall, the ANOVA confirms that process intensification consistently enhances chlorine-mediated oxidation performance (see Tables S1, S2, S3).

Degradation tests

Once the optimized conditions determined by the experimental design ([NaCl] = 0.88 mol L^{-1} and electric current = 0.78 A) were established, the degradation of the studied pesticides - ametryn, diuron, and hexazinone - was investigated over a reaction time of 60 min for both individual processes (electrochemical, photochemical, and sonochemical) and combined processes (photoassisted electrochemical, sonoelectrochemical, photoassisted sonochemical, and photoassisted sonoelectrochemical).

Based on the data collected from the degradation experiments for each process, graphs showing pH values as a function of reaction time were constructed (Figure 6). From Figure 6 it was observed that the pH values of the treated solutions after the degradation tests ranged from approximately 6.0 to 8.5.

According to Conselho Nacional do Meio Ambiente (CONAMA) Resolution No. 430 of May 13, 2011,[46] which establishes effluent discharge standards, these values remained within the permissible limits, as effluents directly discharged into receiving bodies must have a pH between 5 and 9. These values also comply with the limits set by Federal Consolidation Ordinance No. 5 of September 28, 2017,[47] for water distribution systems, which stipulates a pH range of 6.0 to 9.5.

Observing Figure 6, it can be seen that the pesticide solutions of ametryn, diuron, and hexazinone exhibited pH values between 6.0 and 6.9 up to 20 min of treatment in the processes involving electrolysis (electrochemical, photoassisted electrochemical, sonoelectrochemical, and photoassisted sonoelectrochemical), characterized as acidic solutions, with a tendency toward stabilization between 45 and 60 min of treatment.

For pH values between 3 and 8, the predominant species is hypochlorous acid (HOCl), which exhibits a stronger germicidal effect than the hypochlorite ion (ClO^-), since HOCl remains undissociated at pH below 6.5.[48-50] For pH above 8, the prevailing species is hypochlorite (ClO^-).[48,49] Furthermore, under acidic conditions (pH 4.5-6.5), the oxidation of organic compounds occurs more rapidly and efficiently when mediated by active chlorine species compared to alkaline conditions.[51,52]

Thus, it can be inferred that up to 20 min of treatment, the presence of HOCl species was detected in the processes involving electrolysis, which likely contributed to accelerating the degradation of the studied pesticides. In the processes that did not involve electrolysis (photochemical, sonochemical, and photoassisted sonochemical), the pH of the solutions ranged between 5.9 and 6.8, but no production of FCS, mainly ClO^-, was observed, as electrolysis is responsible for generating these species, showing a tendency toward stabilization after 30 min of treatment.

To further investigate the production of free chlorine species ($HOCl/OCl^-$) in the solution, chlorine concentration versus reaction time plots were constructed for each pesticide and process (Figure 7).

Analyzing Figure 7, it is evident that FCS production occurred in the electrochemical, sonoelectrochemical, photoassisted electrochemical, and photoassisted sonoelectrochemical processes, all of which involved electrolysis - the primary mechanism responsible for generating FCS. Consequently, the photochemical, sonochemical, and photoassisted sonochemical processes did not exhibit FCS production.

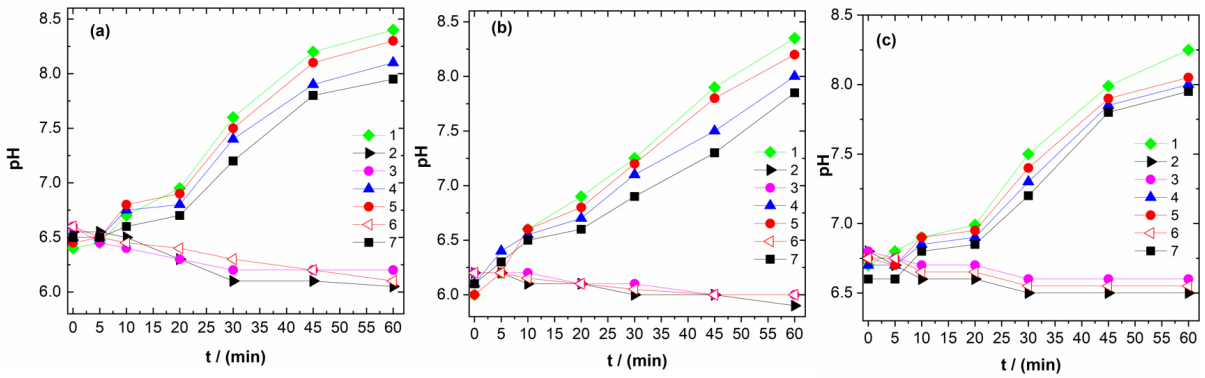

Figure 6. Evolution of pH as a function of reaction time during the degradation of (a) ametryn, (b) diuron, and (c) hexazinone under different treatment processes: (1) EC; (2) UV; (3) US; (4) EC/UV; (5) EC/US; (6) UV/US; and (7) EC/UV/US. Initial pesticide concentration = 20 mg L^{-1}; [NaCl] = 0.88 mol L^{-1}. EC: electrochemical UV: photochemical, and US: sonochemical techniques.

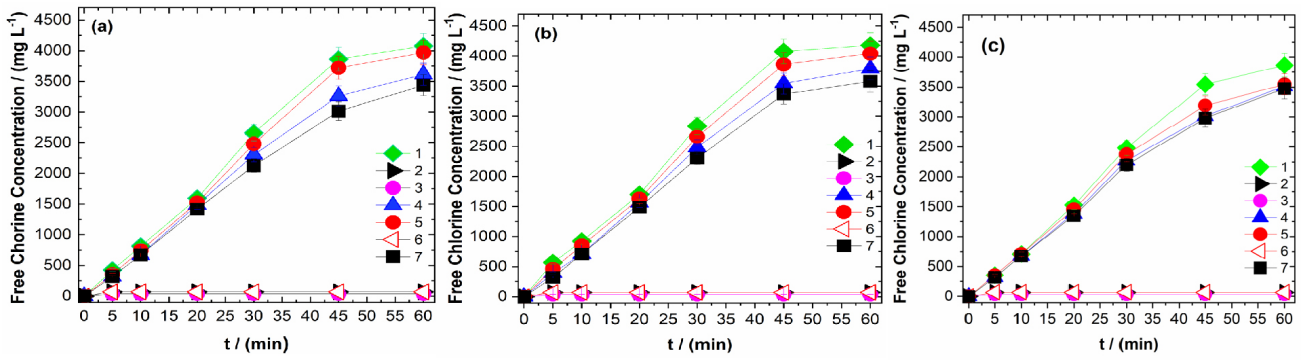

Figure 7. Concentration of free chlorine species ($HOCl/OCl^-$) as a function of reaction time during the degradation of (a) ametryn, (b) diuron, and (c) hexazinone for the different treatment processes: (1) EC; (2) UV; (3) US; (4) EC/UV; (5) EC/US; (6) UV/US; and (7) EC/UV/US. FCS formation is observed only in processes involving electrolysis. EC: electrochemical UV: photochemical, and US: sonochemical techniques.

The concentration of chlorine produced increased with reaction time, showing a tendency toward stabilization between 45 and 60 min of electrolysis. A more detailed analysis revealed that up to 20 min of treatment, the concentrations of FCS generated by these processes were nearly equivalent. After 20 min, higher concentrations of these species were detected in the electrochemical process, followed by the sonoelectrochemical, photoassisted electrochemical, and photoassisted sonoelectrochemical processes, for all three pesticides studied - ametryn, diuron, and hexazinone.

Although direct mechanistic tools such as electron paramagnetic resonance (EPR) spectroscopy or radical scavenging assays were beyond the experimental scope of this work, the mechanistic interpretation was supported by quantitative monitoring of free chlorine species ($HOCl/OCl^-$) and by pH-dependent speciation analyses (Figures 6 and 7). These measurements allowed indirect verification of the generation of reactive chlorine intermediates ($Cl^{\bullet}$, $Cl_2^{\bullet-}$) and hydroxyl radicals (•OH), which are expected during NaCl electrolysis under UV and ultrasound activation. The key chlorine-mediated pathways relevant to this study are described by equations 9-11. Equation 9 presents the anodic oxidation of chloride to molecular chlorine:

$$2Cl^-_{(aq)} \rightarrow Cl_{2(g)} + 2e^- \quad (9)$$

The rapid hydrolysis of Cl_2 to hypochlorous acid (HOCl) subsequently occurs and is given in equation 10.

$$Cl_{2(g)} + 2H_2O_{(l)} \rightarrow HOCl_{(aq)} + 2Cl^-_{(aq)} + H^+_{(aq)} \quad (10)$$

The subsequent acid-base equilibrium between HOCl and hypochlorite (OCl^-) (equation 11), is governed by solution pH.

$$HOCl_{(aq)} \rightleftharpoons H^+_{(aq)} + ClO^-_{(aq)} \quad (11)$$

These reactions provide a direct mechanistic framework for interpreting the experimental trends observed. During the first 20 min of treatment, the solution remained mildly acidic (pH 6.0-6.9), favoring HOCl as the dominant oxidizing species, which explains the faster degradation rates and the steep initial increase in FCS observed in Figure 7. As the pH gradually approached neutral values, the equilibrium described in equation 11 shifted toward OCl^-, a weaker oxidant, consistent with the stabilization of chlorine concentrations and the slower degradation rates observed at later treatment times. Thus, the formation and speciation of active chlorine species predicted by equations 9-11 are fully consistent with the measured pH profiles and chlorine production curves, providing a clear mechanistic basis for the degradation behavior observed in all electrolysis-based processes.

According to Ren *et al.*,[53] Zhang *et al.*,[54] and Yaghoot-Nezhad *et al.*,[55] during NaCl electrolysis, oxygen transfer reactions involving adsorbed oxychlorinated intermediates can simultaneously generate active chlorine species through reactive oxygen species (ROS). UV irradiation, as described by Peng *et al.*[56] and Wu *et al.*,[57] promotes the cleavage of chemical bonds, thereby enhancing FCS generation. Additionally, ultrasound (US) irradiation induces bond breakage in target compounds, causing thermal dissociation and homolytic cleavage of molecules in solution, as reported by Devos *et al.*[58] and Fuentes-García *et al.*[59]

High performance liquid chromatography (HPLC)

The concentration data of the studied pesticides, ametryn, diuron and hexazinone, as a function of time, for the electrochemical, photochemical, sonochemical, photoassisted electrochemical, sonoelectrochemical, photoassisted sonochemical and photoassisted sonoelectrochemical processes are given in Figure 8.

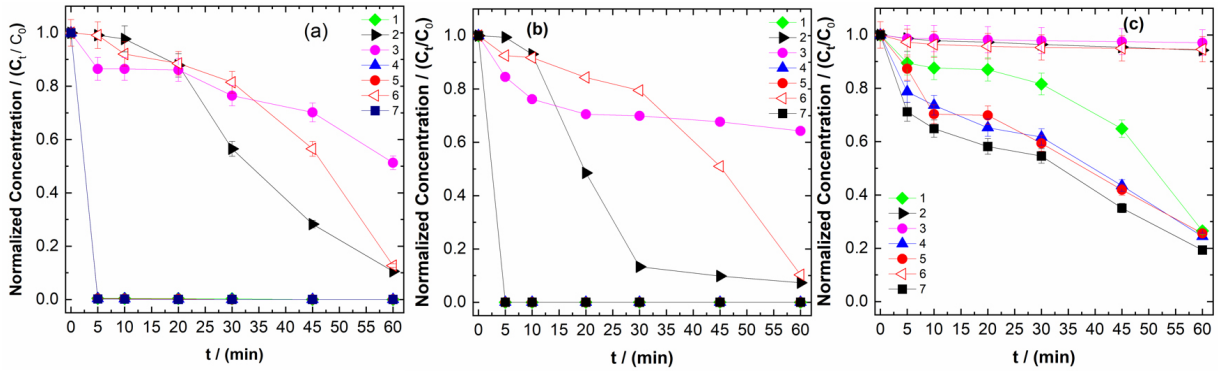

Figure 8. Normalized concentration profiles (C/C_0) of (a) ametryn, (b) diuron, and (c) hexazinone as a function of reaction time obtained by HPLC analysis for the following processes: (1) EC; (2) UV; (3) US; (4) EC/UV; (5) EC/US; (6) UV/US; and (7) EC/UV/US. Initial concentration = 20 mg L^{-1}; reaction time = 60 min. EC: electrochemical UV: photochemical, and US: sonochemical techniques.

Observing Figure 8, it is possible to note the reduction in the concentrations of ametryn, diuron, and hexazinone across all evaluated processes. HPLC quantification was based on calibration curves with correlation coefficients $R^2 > 0.995$, limits of detection (LOD) between 0.3 and 0.6 mg L^{-1}, and triplicate injections for each sample. The inclusion of these analytical parameters strengthens the reliability of the degradation trends observed and ensures accurate interpretation of the concentration profiles.

The percentage removal values for all seven processes (electrochemical, photochemical, sonochemical, photoassisted electrochemical, sonoelectrochemical, photoassisted sonochemical, and photoassisted sonoelectrochemical) are presented in Table 4.

Table 4. Percentage removal of ametryn, diuron, and hexazinone after 60 min of treatment under different individual and combined oxidation processes

Process	Removal / %		
	Ametryn	Diuron	Hexazinone
Electrochemical	ca. 100	ca. 100	70.5
Photochemical	89.8	88.7	6.1
Sonochemical	48.7	35.7	2.8
Photoassisted electrochemical	ca. 100	ca. 100	75.1
Sonoelectrochemical	ca. 100	ca. 100	74.4
Photoassisted sonochemistry	87.1	85.2	5.4
Sonoelectrochemical photoassisted	ca. 100	ca. 100	80.7

Initial pesticide concentration = 20 mg L^{-1}; optimized conditions for electrochemical processes: [NaCl] = 0.88 mol L^{-1} and applied current = 0.78 A. Values reported as approximate removals based on HPLC quantification.

Consistent with the removal data summarized in Table 4, the electrochemical, electrochemical-photoassisted, sonoelectrochemical, and sonoelectrochemical-photoassisted processes rapidly reduced ametryn and diuron concentrations to below the LOD within the first 5 min of treatment, achieving removals close to 100%. Hexazinone, due to its distinct physicochemical properties, exhibited lower reactivity, showing a less pronounced decrease compared to ametryn and diuron-particularly in the photochemical, sonochemical, and photoassisted sonochemical processes. For the same electrochemical-based routes, hexazinone removals ranged from 70.5 to 80.7% after 60 min.

The addition of UV and ultrasound significantly enhanced the removal efficiency for all pesticides relative to the individual photo- and sonochemical processes.

In the degradations by electrochemical, photoassisted electrochemical, sonoelectrochemical and photoassisted sonoelectrochemical processes, from 5 min onwards the concentrations of treated solutions of ametryn and diuron were below the limit of detection, which means a removal of these pesticides of approximately 100%. For hexazinone, a removal rate of 70.5, 75.1, 74.4 and 80.7% was achieved in 60 min of treatment, by these same processes, respectively. Emphasizing that hexazinone interacts differently in relation to diuron and ametryn, probably due to its specific characteristics and physicochemical properties, such as molecular structure, solubility, partition coefficient, among others.

These results are consistent with the maximum allowable levels for the herbicides ametryn and diuron in water intended for human consumption, according to the drinking water standards of Brazil,[60] the United States,[61] and the guideline values established by the World Health Organization (WHO)[62] and Canada,[63] with the exception of the pesticide hexazinone, whose concentration in the treated solution exceeded the established limit ($> 1.4 \times 10^{-6}$ mol L^{-1}).

Furthermore, when comparing the oxidation of the pesticides ametryn, diuron, and hexazinone, it is observed that ametryn and diuron are more readily oxidized than

hexazinone. According to Sanchez-Castrillon *et al.*[51] and Randazzo *et al.*,[52] this may be related to the effect of different oxidants generated during the chemical reactivity of organic compounds. These species can be produced from ions present in the effluent solutions, allowing each organic compound to be attacked with varying efficiency depending on its chemical structure. Additionally, it is worth noting that some chemical and physical processes may occur more rapidly, as reported by Delgado-Vargas and Giraldo-Aguirre[64] and Oliver *et al.*[65]

A mechanistic interpretation was developed to relate the molecular descriptors to the reactivity patterns observed for ametryn, diuron, and hexazinone. As described in the literature, ametryn (solubility: 209 mg L^{-1}) and diuron (42 mg L^{-1}) exhibit substantially lower water solubility and higher hydrophobicity (higher log K_ow) compared to hexazinone (33,000 mg L^{-1}).[66] These physicochemical properties promote partitioning into hydrophobic domains and impose diffusion limitations near the electrode surface, resulting in slower degradation in processes where mass transfer governs the availability of the pollutant to reactive species such as $^{\bullet}OH$ and $Cl^{\bullet}$.

In contrast, the extremely high solubility and lower log K_ow of hexazinone enable faster transport in the aqueous phase, allowing more efficient interaction with both electrochemically generated oxidants and radicals formed through photochemical or sonochemical pathways. This structure-reactivity relationship explains the selective behavior observed in the kinetic data and reinforces that solubility and hydrophobicity play a decisive role in determining pesticide susceptibility to advanced oxidation processes.

Total organic carbon (TOC)

The TOC values were calculated stoichiometrically based on the carbon fraction in the molecular formula of each pesticide (Table 5) and on the initial concentration of the prepared solutions. These values were used as the initial reference (TOC_0) to determine the mineralization efficiency of the system. Using the theoretical TOC ensures that the calculated removal percentage reflects the maximum possible mineralization relative to the mass of contaminant added, eliminating instrumental variations in the initial measurement.

Table 5. Molecular formula, molar mass, and theoretical total organic carbon (TOC_0) values calculated for the initial aqueous solutions of ametryn, diuron, and hexazinone. TOC_0 values were determined stoichiometrically based on the carbon content of each molecule and the initial pesticide concentration

	Ametryn	Diuron	Hexazinone
Molecular formula	$C_9H_{17}N_5S$	$C_9H_{10}Cl_2N_2O$	$C_{12}H_{20}N_4O_2$
Molecular mass / (g mol^{-1})	227.33	233.09	252.31
TOC theoretical / (mg L^{-1})	9.50	9.27	11.41

Figure 9 shows the TOC values removed at the end of the degradation treatments of the studied pesticides, ametryn, diuron, and hexazinone, for the sonochemical, photochemical, photoassisted sonochemical, electrochemical, photoassisted electrochemical, sonoelectrochemical, and photoassisted sonoelectrochemical processes, with the degradation time (0-90 min) displayed on the *x*-axis for each process and pesticide.

Comparing the solutions treated by each process, it can be seen in Figure 9 that the photoassisted sonoelectrochemical process presented a higher TOC removal value compared to the other processes, with 91, 94 and 77% for ametryn, diuron and hexazinone, respectively. Hexazinone had a lower TOC removal value compared to ametryn and diuron, but it was significant. This fact may be related to the lower production of FCS for hexazinone and, consequently,

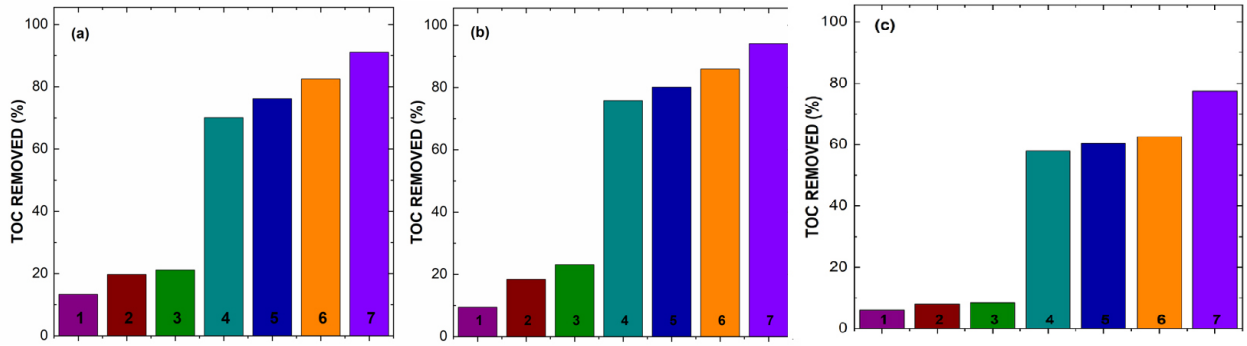

Figure 9. Total organic carbon (TOC) removal as a function of reaction time for (a) ametryn, (b) diuron, and (c) hexazinone under different oxidation processes: (1) US; (2) UV; (3) UV/US; (4) EC; (5) EC/UV; (6) EC/US; and (7) EC/UV/US. TOC values are expressed relative to the theoretical initial TOC calculated from the molecular composition of each pesticide. EC: electrochemical UV: photochemical, and US: sonochemical techniques.

lower generation of highly oxidizing species, the hydroxyl radicals, responsible for acting in the removal/degradation of this pesticide.

From the TOC concentration data for each pesticide studied, ametryn, diuron and hexazinone, to determine the synergistic effect of the photoassisted sonoelectrochemical process, the kinetic analysis of the photoassisted electrochemical, photochemical, sonochemical and photoassisted sonoelectrochemical processes was performed, obtaining the constants kinetics (k) of these processes, as well as the linear regression coefficients (R^2), as shown in Table 6.

The pseudo-first-order kinetic model was selected because, in higher-order kinetic systems involving complex organic degradation pathways, reactions often exhibit apparent first-order behavior under typical operating conditions. In the present study, comparative tests were performed using both first- and second-order models to identify the best fit. The pseudo-first-order model provided the most accurate representation of the removal behavior, yielding higher linear regression coefficients ($R^2 > 0.97$) than the second-order model.

This diagnostic comparison is presented in Figure 10, where the linearity of $\ln(C/C_0)$ *versus* time confirms the suitability of the model for describing the degradation process. The kinetic behavior is further supported by mechanistic considerations: the high chloride concentration in the electrolyte and the continuous-flow operation enhance mass-transfer conditions, promoting an apparent first-order response, as previously reported by Ghanbarlou *et al.*,[67] Pedersen *et al.*,[68] and Raut-Jadhav *et al.*[69]

Although Arrhenius analysis and activation energy estimation were not performed due to the isothermal experimental setup, the revised text provides an explicit and scientifically grounded justification for the adopted kinetic framework. Moreover, the kinetic treatment employed here follows the same methodological rigor reported by Tonhela *et al.*,[26] who also observed pseudo-first-order kinetics and evaluated associated parameters such as E_{EO} and current efficiency in combined EC/UV/US systems.

In addition, the fact of adding NaCl to the reaction mixture in a larger amount, associated with the mode of operation of the continuous flow system, favoring the mass transport, may have conferred kinetic characteristics of a pseudo-first order model.[67-69]

To define the synergy of the photoassisted sonoelectrochemical process, the synergistic coefficient (Sc) was

Table 6. Pseudo-first-order kinetic parameters for the degradation of ametryn, diuron, and hexazinone under electrochemical (EC), photochemical (UV), sonochemical (US), and photoassisted sonoelectrochemical (EC/UV/US) processes

Process	Kinetic data	Ametryn	Diuron	Hexazinone
Electrochemical	k / min^{-1}	7.13×10^{-2}	1.40×10^{-1}	6.99×10^{-3}
	R^2	0.9936	0.9978	0.9869
Photochemical	k / min^{-1}	4.90×10^{-3}	6.40×10^{-3}	2.70×10^{-3}
	R^2	0.9888	0.9898	0.9848
Sonochemical	k / min^{-1}	5.10×10^{-3}	2.60×10^{-3}	2.20×10^{-3}
	R^2	0.9899	0.9985	0.9876
Photoassisted sonoelectrochemical	k / min^{-1}	2.41×10^{-1}	2.85×10^{-1}	1.80×10^{-2}
	R^2	0.9991	0.9993	0.9975

K: apparent rate constant; R^2: linear regression coefficient.

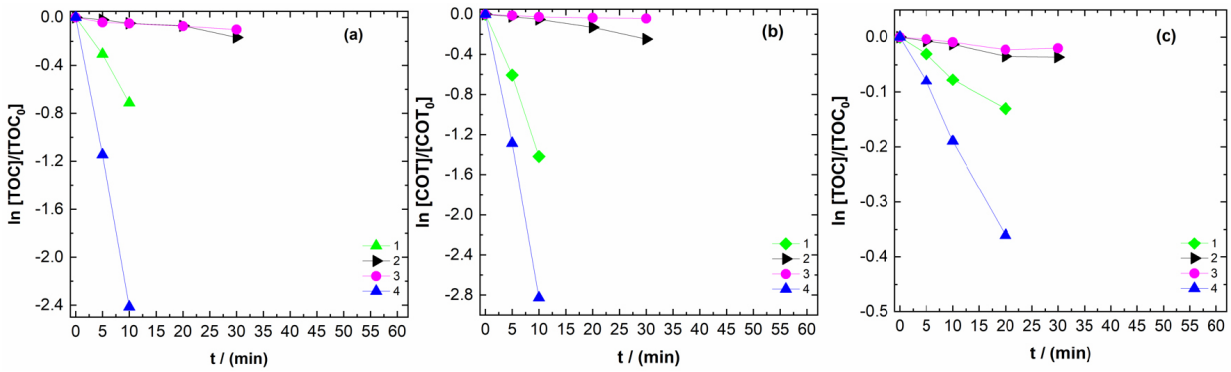

Figure 10. Pseudo-first-order kinetic plots of $\ln(C/C_0)$ *versus* reaction time for (a) ametryn, (b) diuron, and (c) hexazinone obtained under the following processes: (1) EC; (2) UV; (3) US; and (4) EC/UV/US, confirming first-order degradation behavior. EC: electrochemical UV: photochemical, and US: sonochemical techniques.

calculated from the TOC data, since all degradation reactions by the photoassisted electrochemical, photochemical, sonochemical and photoassisted sonoelectrochemical processes adjusted well to the kinetic model of pseudo-first order. Thus, the synergistic coefficient was obtained, being ca. 3.0 for ametryn, ca. 2.0 for diuron and ca. 1.5 for hexazinone.

Evaluating the results of the kinetic and synergistic analysis, it is verified that the removal by the photoassisted sonoelectrochemical process occurred more quickly, compared to the individual processes, for the pesticide diuron, followed by ametryn and hexazinone. According to Pedersen *et al*.,[68] this fact can be explained by the greater affinity of the reaction in relation to hydroxyl radicals, of the pesticides diuron and ametryn in comparison to hexazinone. Furthermore, the slower removal rate for hexazinone may indicate mass transfer limitation.[67]

The combined process, photoassisted sonoelectrochemical, presented synergistic behavior for the three pesticides. The greatest synergistic effect was observed for the pesticides ametryn and diuron, which had similar removal rates, with hexazinone showing less synergy. This synergy difference can be attributed to the specific characteristics of the target compound, such as the molecular structure of the compound, functional groups and physicochemical properties.[69]

Thus, why hexazinone interacts differently, compared to ametryn and diuron, may be associated with different molecular structure, greater solubility (1.31×10^{-1} mol L^{-1}), compared to ametryn (9.2×10^{-4} mol L^{-1}) and diuron (1.8×10^{-4} mol L^{-1}), and lower partition coefficient ($\log k_{ow} = 2.20$), compared to ametryn ($\log k_{ow} = 2.98$) and diuron ($\log k_{ow} = 2.68$).[70]

Thus, the synergistic effect observed for the photoassisted sonoelectrochemical process, more expressive for the pesticides ametryn and diuron, showed an increase in the rate of dissociation of NaCl to generate a greater amount of highly oxidizing radicals, the hydroxyl radicals. In addition, the combination of these processes also contributed to increase the conductivity and diffusivity in the reaction medium, promoting the effective use of hydroxyl radicals by pollutant molecules.

The synergistic effect and the higher yield resulting from the combination of processes can be attributed to the increased conversion of organic by-products into simpler final products, such as CO_2 and H_2O, according to Raut-Jadhav *et al*.[69]

To estimate the feasibility of the photoassisted sonoelectrochemical process, the parameter electrical energy by order (E_{EO}) was calculated, whose values of electrical energy by order (EEO) and the model adjustment, represented by the regression coefficient linear (R^2) and kinetic constant (k) are shown in Table 7.

Observing the data in Table 7, there was a good fit of the first-order kinetic model for all degradation reactions by electrochemical, photoassisted electrochemical, sonoelectrochemical and photoassisted sonoelectrochemical processes, due to the satisfactory values of the linear regression coefficients (R^2). Emphasizing that tests were performed for the first and second order kinetic models, to compare and determine the best fit.

The lowest values of electrical energy *per* order (E_{EO}) were obtained by the photoassisted sonoelectrochemical process for the three pesticides studied, ametryn (4.02 kWh m^{-3} $order^{-1}$), diuron (3.35 kWh m^{-3} $order^{-1}$) and hexazinone (43.77 kWh m^{-3} $order^{-1}$), which presented the highest values of the kinetic constant (k) (Table 7).

According to Alves *et al*.,[71] the lower the EEO, the greater the pollutant removal efficiency in terms of electrical energy consumption. Given these results, the photoassisted sonoelectrochemical process proved to be efficient, in terms of electrical energy, in the degradation of the studied pesticides.

Therefore, the TOC results for the studied pesticides, ametryn, diuron and hexazinone indicated a more evident reduction in the TOC content by the photoassisted sonoelectrochemical process, demonstrating the effectiveness of this process for these pesticides.

Table 7. Electrical energy *per* order (E_{EO}), pseudo-first-order rate constants (k), and regression coefficients (R^2) for the degradation of ametryn, diuron, and hexazinone in processes involving electrolysis. EEO values quantify the electrical energy required to reduce contaminant concentration by one order of magnitude

Process	Ametryn			Diuron			Hexazinone		
	R^2	k / s^{-1}	E_{EO} / (kWh m^{-3} $order^{-1}$)	R^2	k / s^{-1}	E_{EO} / (kWh m^{-3} $order^{-1}$)	R^2	k / s^{-1}	E_{EO} / (kWh m^{-3} $order^{-1}$)
EC	0.9936	7.13×10^{-2}	18.38	0.9978	1.40×10^{-1}	7.76	0.9869	6.99×10^{-3}	86.04
EC/UV	0.9943	8.52×10^{-2}	12.09	0.9921	1.90×10^{-1}	5.12	0.9930	1.67×10^{-2}	71.64
EC/US	0.9931	7.08×10^{-2}	15.18	0.9956	1.61×10^{-1}	6.63	0.9909	1.59×10^{-2}	78.39
EC/UV/US	0.9991	2.41×10^{-1}	4.02	0.9993	2.85×10^{-1}	3.35	0.9975	1.80×10^{-2}	43.77

EC: electrochemical UV: photochemical, and US: sonochemical techniques.

Additionally, the significant synergistic effect presented by the photoassisted sonoelectrochemical process demonstrates a pronounced influence of this combined technique in the removal of these studied pesticides. In addition, the analysis of the parameter electrical energy by order (EEO) demonstrated the feasibility of the photoassisted sonoelectrochemical process in the degradation of the studied pesticides.

Energy analysis

Current efficiency (CE), energy consumption (EC) and energy efficiency (EE) analyzes were performed for the processes that employed electrolysis, as a function of FCS, with the average values shown in Table 8.

The EC was calculated by means of the TOC data, the EC was determined by the cell potential measurements, and by the FCS values, the energy efficiency (EE) was obtained.

Despite the high removal percentages achieved by the triple-combined system, the CE values reported in Table 8 remain relatively low. This behavior is commonly observed in electrochemical systems operating at high current densities and is primarily attributed to two competing phenomena. First, a significant oxygen evolution reaction (OER) occurs at the anode ($2H_2O \rightarrow O_2 + 4H^+ + 4e^-$), consuming a portion of the applied electrical charge that would otherwise contribute to pollutant degradation. Second, electrochemical oxidation can lead to the formation of partially converted, stable intermediates (such as refractory chlorinated compounds), which exhibit slower mineralization kinetics than the parent pesticides. Nevertheless, the energy consumption and current-efficiency findings are consistent with values reported in the literature for similar DSA-based systems optimized through factorial design, as demonstrated by Tonhela *et al*.[26]

An analysis of the values contained in Table 8 shows a higher EC value by the photoassisted sonoelectrochemical process for the three pesticides studied, ametryn (5.13%), diuron (5.28%) and hexazinone (4.65%) when compared to the other processes, since this process presented a greater removal of TOC for these pesticides, confirming the effect of the association of the three processes (electrochemical, photochemical and sonochemical).

Still observing Table 8, there is the lowest EC value when using the photoassisted sonoelectrochemical process for the three pesticides, ametryn (25.37 kWh m^{-3}), diuron (24.65 kWh m^{-3}) and hexazinone (28.40 kWh m^{-3}), which had the lowest cell potential values.

In addition to the electrical energy *per* order (E_{EO}) calculated for the electrochemical contribution, the total energy demand of the integrated photoassisted sonoelectrochemical process was also evaluated. This included the power consumption of the UV lamp (375 W), the ultrasonic bath (60 W), and the electrochemical cell operating at 0.78 A and 10 V. Therefore, the overall energy required *per* treatment cycle corresponds to the sum of these three contributions. The revised text now integrates this complete energy assessment into the discussion of EEO, CE, and EE, supported by the data presented in Table 8. This expanded evaluation allows a more realistic estimation of operational costs and confirms the superior energy performance of the combined process.

According to Fernandes *et al*.,[72] Pérez *et al*.,[73] and Dolatabadi *et al*.,[74] the decrease in cell potential is associated with a good conductivity of the medium, resulting in reduced energy consumption and increased system efficiency, and consequently, causing EE in terms of satisfactory FCS production in the degradation of ametryn (85.47%), diuron (87.77%) and hexazinone (83.14%), by this process.

Conclusions

This study demonstrates the relevance of advanced treatment technologies for industrial effluents and wastewaters and highlights the importance of appropriate process planning based on robust statistical design. Such an approach reduces experimental time, reagent consumption,

Table 8. Current efficiency (CE), energy consumption (EC), and energy efficiency (EE) values calculated for the electrochemical-based processes as a function of free chlorine species (FCS) generation during the degradation of ametryn, diuron, and hexazinone

Process	Ametryn			Diuron			Hexazinone		
	CE / %	EC / (kWh m^{-3})	EE / %	CE / %	EC / (kWh m^{-3})	EE / %	CE / %	EC / (kWh m^{-3})	EE / %
EC	3.79	29.64	98.80	3.91	28.86	99.67	3.31	32.44	91.61
EC/UV	4.51	27.46	87.63	4.79	26.21	91.53	4.03	30.58	85.94
EC/US	4.10	28.39	96.23	4.32	27.92	97.48	3.89	30.94	86.87
EC/UV/US	5.13	25.37	85.47	5.28	24.65	87.77	4.65	28.40	83.14

EC: electrochemical UV: photochemical, and US: sonochemical techniques.

and waste generation, in line with the principles of Green Chemistry. Experimental design allowed the identification of optimal operational conditions for free chlorine species generation ([NaCl] = 0.88 mol L^{-1} and applied current = 0.78 A), which were subsequently employed in the degradation experiments.

Monitoring of the pH showed that the treated solutions of ametryn, diuron, and hexazinone remained within regulatory limits throughout the experiments. For electrolysis-based processes, the pH ranged from 6.0 to 6.9 during the first 20 min of treatment, favoring the predominance of hypochlorous acid (HOCl), which contributed to the enhanced degradation rates observed under these conditions. HPLC analyses revealed high removal efficiencies for the photo-assisted sonoelectrochemical process, achieving nearly complete removal of ametryn and diuron and 80.7% removal of hexazinone. Consistently, TOC measurements indicated substantial mineralization, with reductions of 91% for ametryn, 94% for diuron, and 77% for hexazinone.

The combined HPLC and TOC results confirm the superior performance of the photo-assisted sonoelectrochemical process in both degradation and mineralization of the studied pesticides. The pronounced synergistic effect observed for this coupled system, together with favorable electrical E_{EO} values, demonstrates its technical and energetic feasibility. Overall, the photo-assisted sonoelectrochemical process proved to be an effective, economically viable, and promising strategy for the treatment of effluents containing ametryn, diuron, and hexazinone.

Supplementary Information

Supplementary data (ANOVA tables) are available free of charge at http://jbcs.sbq.org.br as a PDF file.

Data Availability Statement

The data supporting the findings of this study are available within the manuscript and its SI section.

Acknowledgments

This work was funded by FAPEMIG, CNPq and CAPES. Artificial intelligence-based tools were used to assist with language revision and textual organization of the manuscript. No AI tools were used for data generation, data analysis, or interpretation of the results. All scientific decisions and conclusions were made exclusively by the authors

Author Contributions

K.S.A. was responsible for conceptualization, data curation, investigation, writing original draft; B.S. for investigation, writing original draft; M.A.T. for conceptualization, data curation, investigation, M.E.V. and M.S.F. for investigation; A.C.G. for conceptualization, data curation; A.L.S.A. and D.C.F. for writing-review and editing; G.R.P.M. for conceptualization, data curation, formal analysis, project administration, resources, writing (original draft, review and editing).

References

1. Yadav, P.; Chivate, M. S.; Yadav, V. K.; Mishra, V.; *Bioresour. Technol. Rep.* **2025**, *31*, 102295. [Crossref]
2. Carvalho, R.; Guedes, P.; Mateus, E. P.; Silva, V.; Tyrologou, P.; Koukouzas, N.; Ribeiro, A. B.; Couto, N.; *Open Res. Eur.* **2025**, *5*, 257. [Crossref]
3. Pathak, V. M.; Pathak, R.; Kumar, A.; *Front Microbiol.* **2022**, *29*, 87467. [Crossref]
4. Yu, Y.; Wang, Z.; Yao, B.; Zhou, Y.; *Sci. Total Environ.* **2024**, *923*, 171388. [Crossref]
5. Kalyabina, V. P.; Esimbekova, E. N.; Kopylova, K. V.; Kratasyuk, V. A.; *Toxicol. Rep.* **2021**, *8*, 1179. [Crossref]
6. Shekhar, C.; Khosya, R.; Thakur, K.; Mahajan, D.; Kumar, R.; Kumar, S.; Sharma, A. K.; *Toxicol. Rep.* **2024**, *13*, 101840. [Crossref]
7. Nagy, K.; Duca, R. C.; Lovas, S.; Creta, M.; Scheepers, P. T. J.; Godderis, L.; Ádám, B.; *Environ. Res.* **2020**, *181*, 108926. [Crossref]
8. Felicio, A. L. S. M.; Monteiro, A. M.; Almeida, M. B.; Madeira, T. B.; Nixdorf, S. L.; Yabe, M. J. S.; *An. Acad. Bras. Cienc.* **2016**, *88*, 1235. [Crossref]
9. Huang, Y.; Li, Z.; *iScience* **2025**, *28*, 112861. [Crossref]
10. Lorenz, S.; Trau, F. N.; Ruf, L. C.; Meinikmann, K.; Fisch, K.; Stähler, M.; Schenke, D.; Blevins, H. L.; Heinz, M.; *Sci. Total Environ.* **2025**, *975*, 179250. [Crossref]
11. Cossu, L. O.; Al-Hamadani, Y. A. J.; *ACS EST Water* **2024**, *4*, 3629. [Crossref]
12. Syafrudin, M.; Kristanti, R. A.; *Int. J. Environ. Res. Public Health* **2021**, *18*, 468. [Crossref]
13. Dagnew, M.; Xue, Q.; Zhang, J.; Wang, Z.; Zhou, A.; Li, M.; Zhao, C.; *Sustainability* **2025**, *17*, 4710. [Crossref]
14. Khurshid, S.; Kumar, S.; Kumar, D. R.; Quaff, A. R.; Jha, R.; Wipulanusat, W.; *Green Technol. Sustainability* **2026**, *4*, 100254. [Crossref]
15. Silva, C. I.; Ribeiro, K. S.; *Rev. Gestão Secretariado* **2024**, *15*, 4220. [Crossref]
16. Saleh, I. A.; Zouari, N.; Al-Ghouti, M. A.; *Environ. Technol. Innov.* **2020**, *19*, 101026. [Crossref]
17. Ahmed, M. B.; Zhou, J. L.; Ngo, H. H.; Guo, W.; Thomaidis,

N. S.; Xu, J.; *J. Hazard. Mater.* **2016**, *323*, 274. [Crossref]
18. Peralta-Hernández, J. M.; Brillas, E.; *Sep. Purif. Technol.* **2025**, *378*, 134737. [Crossref]
19. Kanakaraju, D.; Glass, B. D.; Goh, P. S.; *Environ. Sci. Pollut. Res.* **2025**, *32*, 14316. [Crossref]
20. Khan, Z. U. H.; Sabahat, S.; Shah, N. S.; Ajab, H.; Iqbal, J.; Ullah, F.; *J. Water Process Eng.* **2025**, *70*, 107083. [Crossref]
21. Derbalah, A.; Sakugawa, H.; *Int. J. Environ. Res.* **2024**, *18*, 11. [Crossref]
22. Pozeti, G. E. O.: *Análise das Possibilidades e Desafios do Uso de Reator Solar para Remover Pesticidas em Estações de Tratamento de Água*; PhD Thesis, Universidade Estadual Paulista (UNESP), Brazil, 2025. [Link] accessed in January 2026
23. Martínez-Sánchez, C.; Robles, I.; Godínez, L. A.; *Int. J. Environ. Sci. Technol.* **2022**, *19*, 12611. [Crossref]
24. Deshmukh, N. S.; Deosarkar, M. P.; *Mater. Today: Proc.* **2022**, *57*, 1575. [Crossref]
25. Frigulio, M. A. P.; Valério, A. S.; Forti, J. C.; *Processes* **2025**, *13*, 2227. [Crossref]
26. Tonhela, M. A.; Vernillo, N.; Cardoso, L. R.; Almeida, M. E. V.; Malpass, A. C. G.; Malpass, G. R. P.; *Appl. Res.* **2023**, *3*, e202300024. [Crossref]
27. Malpass, G. R. P.; Motheo, A. J.; *Curr. Opin. Electrochem.* **2021**, *27*, 100689. [Crossref]
28. Malpass, G. R. P.; Motheo, A. J.; *J. Appl. Electrochem.* **2001**, *31*, 1351. [Crossref]
29. Tonhela, M. A.; Almeida, M. E. V.; Malpass, A. C. G.; Motheo, A. J.; Malpass, G. R. P.; *Environ. Technol.* **2023**, *44*, 1782. [Crossref]
30. Antonelli, R.; Malpass, G. R. P.; da Silva, M. G. C.; Vieira, M. G. A.; *J. Water Process Eng.* **2022**, *47*, 102698. [Crossref]
31. Choi, J.; Cui, M.; Lee, Y.; Kim, J.; Son, Y.; Khim, J.; *Chem. Eng. J.* **2018**, *338*, 323. [Crossref]
32. Weng, M.; Cai, M.; Xie, Z.; Dong, C.; Zhang, Y.; Song, Z.; Shi, Y.; Jin, M.; Wang, Q.; Wei, Z.; *Chem. Eng. J.* **2022**, *431*, 134238. [Crossref]
33. Keen, O.; Bolton, J.; Litter, M.; Bircher, K.; Oppenländer, T.; *Pure Appl. Chem.* **2018**, *90*, 1487. [Crossref]
34. APHA/AWWA/WEF; *Standard Methods for the Examination of Water and Wastewater*, 23rd ed.; American Public Health Association: Washington, DC, 2017.
35. Brondi, S. H. G.; Lanças, F. M.; *J. Liq. Chromatogr. Relat. Technol.* **2004**, *27*, 171. [Crossref]
36. Felicio, A. L. S. M.; Monteiro, A. M.; Almeida, M. B.; Madeira, T. B.; Nixdorf, S. L.; Yabe, M. J. S.; *An. Acad. Bras. Cienc.* **2016**, *88*, 1235. [Crossref]
37. Afify, A. A.; Hassan, G. K.; Al-Hazmi, H. E.; Kamal, R. M.; Mohamed, R. M.; Drewnowski, J.; Majtacz, J.; Makina, J.; El-Gawad, H. A.; *Energies* **2023**, *16*, 4754. [Crossref]
38. Zayas, T.; Vega, M.; Soriano-Moro, G.; Handa, A.; Morales, M.; Salgado, L.; *J. Electrochem. Sci. Technol.* **2024**, *15*, 268. [Crossref]
39. Rodríguez, J. F.; Nava, J. L.; *Chem. Eng. Process.* **2024**, *196*, 109634. [Crossref]
40. Medina Collana, J. T.; Medrano, Y. J. A.; Palomino, L. J. C.; Venegas, L. C.; Dextre, C. A. A.; Meneses, P. A.; Nunez, A. W. P.; *Anal. Bioanal. Electrochem.* **2024**, *16*, 217. [Crossref]
41. Kamel, M.; El-Ashtoukhy, E.-S. Z.; Abdel-Aziz, M. H.; Zahran, R. R.; Sedahmed, G. H.; El Gheriany, I.; *Chem. Eng. Process.* **2022**, *176*, 108959. [Crossref]
42. Janowski, L.; Wroblewski, R.; Dworniczak, J.; Kolakowski, M.; Rogowska, K.; Wojcik, M.; Gajewski, J.; *Sci. Total Environ.* **2021**, *801*, 149712. [Crossref]
43. de Faria, L. B.; Teixeira, G. F.; Alves, A. C. F.; Linares, J. J.; Oliveira, S. B.; Motheo, A. J.; Colmati, F.; *Chem. Eng.* **2023**, *7*, 73. [Crossref]
44. Pose-Juan, E.; Sánchez-Martín, M. J.; Herrero-Hernández, E.; Rodríguez-Cruz, M. S.; *Sci. Total Environ.* **2015**, *536*, 31. [Crossref]
45. Klement, W. J. N.; Savino, E.; Rooijmans, S.; Mulder, P. M. F. A.; Lynn Jr., N. S.; Browne, W. R.; Verpoorte, E.; *ACS Electrochem.* **2025**, *1*, 504. [Crossref]
46. Conselho Nacional do Meio Ambiente (CONAMA); Resolução No. 430, de 13 de maio de 2011, *Dispõe sobre as Condições e Padrões de Lançamento de Efluentes, Complementa e Altera a Resolução No. 357, de 17 de março de 2005, do Conselho Nacional do Meio Ambiente-CONAMA*; 2011. [Link] accessed in January 2026
47. Portaria de Consolidação No. 5 de 28/09/2017. [Link] accessed in January 2026
48. Mehendale, F. V.; Clayton, G.; Homyer, K. M.; Reynolds, D. M.; *J. Glob. Health Rep.* **2023**, *7*, e2023052. [Crossref]
49. Block, M. S.; Rowan, B. G.; *J. Oral Maxillofac. Surg.* **2020**, *78*, 1461. [Crossref]
50. Sil, T. B.; Malyshev, D.; Aspholm, M.; Andersson, M.; *BMC Microbiol.* **2025**, *25*, 101. [Crossref]
51. Sanchez-Castrillon, S.; Benítez, L. N.; Vazquez-Arenas, J.; Ferraro, F.; Palma-Goyes, R. E.; *ACS Omega* **2024**, *9*, 46302. [Crossref]
52. Randazzo, S.; Geagea, A.; Proietto, F.; Galia, A.; Scialdone, O.; *Chemosphere* **2024**, *355*, 141855. [Crossref]
53. Ren, N.; Qu, C.; Zhang, A.; Yu, C.; Li, X.; Meng, S.; *Environ. Sci. Technol.* **2024**, *58*, 22829. [Crossref]
54. Zhang, J.; Su, P.; Xu, T.; Yuan, L.; Qiao, M.; Yang, B.; *Sep. Purif. Technol.* **2023**, *304*, 122408. [Crossref]
55. Yaghoot-Nezhad, A.; Wacławek, S.; Madihi-Bidgoli, S.; Hassani, A.; Lin, K.-Y. A.; Ghanbari, F.; *J. Hazard. Mater.* **2023**, *445*, 130626. [Crossref]
56. Peng, T.; Xu, C.; Yang, L.; Yang, B.; Cai, W.-W.; Gu, F.; Ying, G.-G.; *ACS Omega* **2022**, *7*, 5053. [Crossref]

57. Wu, Y.; Wang, J.; *J. Hazard. Mater.* **2022**, *421*, 126459. [Crossref]
58. Devos, C.; Bampouli, A.; Brozzi, E.; Stefanidis, G. D.; Dusselier, M.; Van Gerven, T.; Kuhn, S.; *Chem. Soc. Rev.* **2025**, *54*, 85. [Crossref]
59. Fuentes-García, J. A.; Santoyo-Salzar, J.; Rangel-Cortes, E.; Goya, G. F.; Cardozo-Mata, V.; Pescador-Rojas, J. A.; *Ultrason. Sonochem.* **2021**, *70*, 105274. [Crossref]
60. Ministério da Saúde; *Portaria GM/MS No. 888*, *de 4 de maio de 2021*; Diário Oficial da União, Brasília, 2021. [Link] accessed in February 2026
61. U.S. Environmental Protection Agency (USEPA); *2018 Edition of the Drinking Water Standards and Health Advisories Tables*; USEPA, Washington, DC, 2018. [Link] accessed in February 2026
62. World Health Organization (WHO); *Guidelines for Drinking-Water Quality, 4th edition, Incorporating the 1st Addendum*. [Link] accessed in January 2026
63. Guidelines for Canadian Drinking Water Quality: Summary Tables. [Link] accessed in January 2026
64. Delgado-Vargas, C. A.; Barreneche-Vasquez, J. S.; González Cógua, N.; Botero-Coy, A. M.; Hernández, F.; Martínez-Pachón, D.; Moncayo-Lasso, A.; *J. Environ. Chem. Eng.* **2023**, *11*, 111030. [Crossref]
65. Oliver, Z. J.; Abrams, D. J.; Cardinale, L.; Chen, C.-J.; Beutner, G. L.; Caille, S.; Cohen, B.; Deng, L.; Diwan, M.; Frederick, M. O.; Harper, K.; Hawkins, J. M.; Lehnherr, D.; Lucky, C.; Meyer, A.; Noh, S.; Nunez, D.; Quasdorf, K.; Teli, J.; Stahl, S. S.; Schreier, M.; *ACS Cent. Sci.* **2025**, *11*, 528. [Crossref]
66. Chiarello, M.; Graeff, R. N.; Minetto, L.; Cemim, G.; Scheider, V. E.; Moura, S.; *Quim. Nova* **2017**, *40*, 158. [Crossref]
67. Ghanbarlou, H.; Pedersen, N. L.; Fini, M. N.; Muff, J.; *Environ. Sci. Pollut. Res.* **2020**, *27*, 22206. [Crossref]
68. Pedersen, N. L.; Fini, M. N.; Molnar, P. K.; Muff, J.; *Sep. Purif. Technol.* **2019**, *208*, 51. [Crossref]
69. Raut-Jadhav, S.; Saharan, V. K.; Pinjari, D.; Sonawane, S.; Saini, D.; Pandit, A.; *J. Hazard. Mater.* **2013**, *261*, 139. [Crossref]
70. National Center for Biotechnology Information (NCBI); *PubChem*. [Link] accessed in January 2026
71. Alves, P. H. L.; Silva, P. S. L.; Ferreira, D. C.; Gonçalves, J. C. S. I.; *Rev. Bras. Recur. Hídricos* **2018**, *23*, e03186. [Crossref]
72. Fernandes, A.; Santos, D.; Pacheco, M. J.; Ciríaco, L.; Lopes, A.; *Sci. Total Environ.* **2016**, *541*, 282. [Crossref]
73. Pérez, G.; Saiz, J.; Ibáñez, R.; Urtiaga, A. M.; Ortiz, I.; *Water Res.* **2012**, *46*, 2579. [Crossref]
74. Dolatabadi, M.; Ehrampoush, M. H.; Pournamdari, M.; Ebrahimi, A. A.; Fallahzadeh, H.; Ahmadzadeh, S.; *Chemosphere* **2023**, *311*, 137001. [Crossref]

Submitted: October 15, 2025
Final version online: February 6, 2026